NASA CONTRACTOR
REPORT

NASA CR-61102

NASA CR-61102

THE MOTION OF ASCENDING AND DESCENDING SPHERES

Prepared Under Contract NAS8-5294 by

Paul B. MacCready, Jr.
Robin E. Williamson

METEOROLOGY RESEARCH, INCORPORATED
Altadena, California

For

NASA - GEORGE C. MARSHALL SPACE FLIGHT CENTER
Huntsville, Alabama

September 13, 1965

NASA CR-61102

THE MOTION OF ASCENDING AND DESCENDING SPHERES

By

Paul B. MacCready, Jr.
Robin E. Williamson

Prepared Under Contract NAS8-5294 by
METEOROLOGY RESEARCH, INCORPORATED
Altadena, California

For

Aerospace Environment Office
Aero-Astrodynamics Laboratory

NASA - GEORGE C. MARSHALL SPACE FLIGHT CENTER

FOREWORD

This report presents the results of a study performed by Meteorology Research, Inc., Altadena, California as part of NASA Contract NAS8-5294 with the Aerospace Environment Office, Aero-Astrodynamics Laboratory, NASA-George C. Marshall Space Flight Center, Huntsville, Alabama. The NASA contract monitor was Mr. James R. Scoggins; Dr. Paul B. MacCready was the principal investigator.

The results of this study improve considerably our understanding of the behaviour of spheres moving through a fluid, but much remains to be done before a complete understanding is achieved.

This report terminates the work on sphere motions as part of the effort on this contract. The contract period covered by this report was April 1964 to December 1964.

TABLE OF CONTENTS

LIST OF ILLUSTRATIONS

LIST OF SYMBOLS

D	Sphere diameter
R_d	Reynolds number = Dx speed/kinematic viscosity (in this report "speed" is taken as instantaneous two-dimensional speed)
C_D	Drag coefficient = $\frac{8\,D^2}{\pi}$ (|buoyancy|)(density)$^{-1}$(speed)$^{-2}$
N, S, L	Sphere roughness element sizes (N, none; S, small; L, large)
(I-I)	Distance between successive lateral accelerations
λ	Wavelength of regular oscillating motion, = 2(I-I)
(SS)	A "Spherical Strouhal" number, = $\frac{D}{2(I\text{-}I)}$; = $\frac{D}{\lambda}$ for regular motion
ymax	Total maximum amplitude of lateral motion in path length λ

THE MOTION OF ASCENDING AND DESCENDING SPHERES

SUMMARY

A series of measurements was made of the self-induced motions of spheres rising or descending in a 35-ft-deep water tank. The trials covered various Reynolds number (R_d) flow regimes, different relative mass (RM) situations (steel descending spheres and light ascending spheres), and different surface roughnesses. At subcritical R_d, smooth and small roughness element spheres gave regular motion (spiral or zigzag). The relative mass effect was consistent with the prediction that the lateral motion total amplitude is proportional to (diameter)$(1 + 2\ RM)^{-1}$.

In all R_d regimes the large roughness element spheres had regular motion of small amplitude.

At critical and supercritical R_d (to 1,250,000), smooth spheres had large irregular wandering motions and spheres with small roughness elements had as great or greater wandering motions.

At high supercritical R_d ($\sim$ 1,600,000) the motion of a smooth sphere reverted to an irregular spiral.

Qualitative observations of the motion suggest that the sphere receives a significant momentum impulse every 7 diameters or so of path length. At subcritical R_d successive impulses are in alternate directions, yielding a fairly regular motion with a wavelength on the order of 14 diameters; at supercritical R_d the impulses are randomly oriented and the resulting motion is a spurious wandering. The various flow regime fundamentals appear analogous to those found in tunnel tests on two-dimensional cylinders. The sphere motions studied in the water tank are not inconsistent with those found for balloons ascending in the atmosphere.

SECTION I. INTRODUCTION

The need for high resolution wind soundings has generated the requirement of understanding the vertical and horizontal motions self-induced by the sounding balloons. The understanding is needed both to interpret data most effectively and to permit optimizing the balloon configuration for soundings.

Meteorology Research, Inc., conducted a survey program probing the self-induced motions of balloons, mostly spherical, and making some simple water tank and atmospheric tests (see MacCready and Jex, 1964). The initial study outlined the main physical factors, helped to define the pertinent Reynolds number regimes and the drag coefficient values typifying each region, demonstrated that the water experiments did agree with air ones, suggested the sort of relative mass effects to be expected, and emphasized the large variety of factors and the large experimental scatter to be found in sphere motion studies.

The present study is a direct outgrowth of the original survey. It is aimed at providing a more systematic and quantitative examination of the factors which dominate the sphere motion picture. The detailed aims include:

(1) Obtaining more accurate data by use of a deeper water tank (to let the spheres reach a representative equilibrium motion) and by use of better data acquisition apparatus.

(2) Paying more attention to the quantitative aspects of the variability of the motion rather than to the mean factors emphasized previously.

(3) Covering a broad R_d range, especially to reach higher R_d and to accent the region just above and just below the critical R_d range.

(4) Studying separately the effects of relative mass (RM, of sphere to fluid) on the amplitude of the self-induced oscillations.

(5) Studying separately the effects of roughness elements (systematically varying element sizes and numbers).

One would like to consider separately the effects on the motion of varying R_d, RM, or roughness with the other two factors being unchanged. Unfortunately, for non-constrained spheres it turns out to be difficult or even impossible to alter only one of these factors at a time. To complicate the matter further, the secondary factors of the details of the release, and of sphericity, minute surface variations, asymmetrical buoyancy, and rotational inertia of the spheres do have roles in determining the sphere motion. This study investigates some quantitative aspects of the motions so as to ascribe magnitudes to the effects of certain factors. However, the great variability of the motions being studied, the large number of variables to be considered, the large variations in motion which can be caused by a small variation of a factor in the critical R_d regime, and the difficulty of altering only one variable at a time all conspire to make this sort of study to be still somewhat in the nature of a survey.

SECTION II. THE TEST SPHERES

Table I summarizes the pertinent information on the 19 spheres used.

TABLE I

SUMMARY OF SPHERES USED ON DATA RUNS

Number	Diameter	RM	Number of Roughness Elements	Height of Roughness Elements	Roughness Category
1	1.63"	7.8	0	-	N
2	1.63	7.8	3*	0.08"	S
3	2.0	7.8	0	-	N
4	3.0	7.8	0	-	N
5	3.0	7.8	many**	0.06	S
6	3.4	0.126	0	-	N
7	3.4	0.119	37	0.05	S
8	3.4	0.136	37	0.19	L
9	5.6	0.153	0	-	N
10	5.6	0.149	82	0.05	S
11	5.6	0.163	82	0.19	L
12	10.5	0.065	0	-	N
13	10.5	0.069	174	0.05	S
14	10.5	0.088	174	0.50	L
15	12.0	0.053	0	-	N
16	12.0	0.052	193	0.05	S
17	12.0	0.065	193	0.50	L
18	16.0	0.037	0	-	N
19	16.0	0.047	254***	0.50	S

*During painting, the surface picked up several patches of sawdust which were then left on.

**The sphere surface was irregularly rough as cast, rather than being smoothed to a typical ball bearing surface.

***Failed structurally.

Most of the spheres are shown in Figures 1, 2, and 3.

Spheres #1 - #5 were steel ball bearings, painted white to make them stand out during the tests. The surface of #5 was "as cast", rather than being smooth. Spheres #6 - #11 were fashioned from hollow plastic toy balls, filled with a foam material (Uralane) to provide rigidity. The water tank tests were made at depths as great as 35 ft which puts a considerable pressure on the spheres. This pressure will compress or otherwise distort the spheres unless they are made rigid. Spheres #12 - #19 were molded hemispheres of high impact styrene about 1/8 inch thick, butt-jointed to form a smooth spherical shell. These hemispheres are ordinarily used for making globes. Each hollow sphere was found to have its center of mass rather closely coinciding with the center of buoyancy. The plastic balls filled with foam-in-place plastic in some cases had the center of mass appreciably away from the center of buoyancy, due to the varying density of the foam material.

For the largest spheres, the buoyant force is great and this requires that special attention be paid to the device which pulls the sphere down to the bottom. A net can conveniently hold down the smooth spheres but will damage and get tangled in the spheres with roughness elements. Therefore, Spheres #13, 14, 16, 17, and 19 had tie points installed which permitted connection to a cable. To spread the load there were two points on opposite sides of the sphere, connected internally by a rod. The buoyancy force on Sphere #19 was so great that the sphere failed structurally.

The roughness elements for the main tests were chosen to provide three distinct roughness conditions: smooth spheres ("N" roughness), small roughness elements ("S") being comparable to or somewhat smaller than the expected boundary layer thickness and large roughness elements ("L") being considerably larger than the boundary layer thickness. The boundary layer thickness was estimated as $2\,\gamma^{1/2} D^{1/2}\,(\text{speed})^{-1/2}$, (where γ is kinematic viscosity). This approximate relation is adapted from standard boundary layer calculations for the subcritical R_d regime, and gives a thickness appropriate for the surface about 75 - 80° around from the front stagnation point. As an example of the three roughness conditions, on Figure 3 Sphere #15 is smooth, Sphere #16 has small roughness elements, and Sphere #17 has large roughness elements. As shown on Figure 3, the large roughness elements employed were short hollow cylinders, chosen because of production simplicity and also to minimize the increase of the sphere's rotational inertia. The small roughness elements were plastic buttons.

SECTION III. EXPERIMENTAL METHOD

General Method

The method chosen for this series of observations was a simple one, directed toward providing primary data economically rather than giving great detail in three dimensions. Two 16 mm movie cameras were used, running at 24 frames per second. One pointed vertically down, looking along the path of the ascending buoyant spheres, while the other pointed horizontally at the intended path from a distance of 32 feet at a depth of 15 feet. The vertical camera showed the detailed lateral sphere motions and also permitted the selection of the portions of the paths for which the horizontal camera data would be most valid (the motion most parallel to the film plane). The quantitative two-dimensional vertical and lateral speed data were obtained with the horizontal camera.

The overall camera setup was a compromise between the need to show a long path length for the largest spheres (at least 10 diameters) and still to resolve the position of the smallest fast-moving metal spheres.

The Facility

For the largest spheres a vertical rise distance of 30 feet was considered the absolute minimum acceptable, to permit the sphere to attain something like a terminal velocity motion and then to be observed for 10 or 15 diameters. There turn out to be few appropriate test facilities of this size. Fortunately, the Bendix Pacific Corp. made available to the project their Sonar Test Tank at the Sylmar Facility.

This tank is 35 ft deep, 40 ft wide, and over 100 ft long. The temperature appeared to be stable at 76°F, but no complete temperature soundings were made during the project. The kinematic viscosity of the water was measured and found to be $0.98 \cdot 10^{-5}$ ft^2 sec^{-1} at 76°F.

Operations

A 14 ft square opening in the steel deck covering the tank was provided as working space for the project. A 600 pound lead weight was lowered to the bottom at the center of this space to serve as an

anchor for the pulley system which was used for the downhaul of the buoyant spheres. The smooth models were released from a sling, the rough models from an eyelet which was small in comparison to the roughness element. The release mechanism was an electrically actuated aircraft bomb shackle which was remotely operated from the surface.

The vertical camera was hand held above the surface near the center point when photographing the positively buoyant models and slightly below the surface with the aid of a water mask for the sinking bodies, since it was anticipated that these would typically have much smaller lateral translations. Marks on the bottom helped provide position reference. Buoyant models were hauled down slowly by means of a pulley system and then an interval of five to ten minutes was allowed for some dissipation of the turbulence which might have been generated.

Data were collected on high speed Ektachrome 16 mm film. Illumination was provided by three 2000-watt underwater gas photo-floods. The time reference was established from the calibrated frame speed of the high-quality cameras. For quantitative data reduction, the film from the horizontal camera was projected and the sequential sphere positions marked relative to fixed markers.

As would be predicted, many of the non-rough spheres had very erratic motion and moved laterally considerable distances. Many test sequences could not be used because the spheres moved outside the range of the cameras or moved so far toward or away from the horizontal camera that the computed velocities would not be accurate since the computations assume the motion to be in the center plane. Throwing out these cases means that the data are somewhat slanted toward the less erratic motions.

SECTION IV. EXPERIMENTAL RESULTS AND INTERPRETATION

The Primary Data

A total of 53 trials were made with Spheres #1 - #18. The data consist of the observers' notes, the qualitative record of the lateral motions obtained with the camera from above, and the quantitative record of the two-dimensional trajectory obtained with the horizontal camera. For each sphere type one or more frame-by-frame plots were made of the sphere trajectory, for simplicity using the assumption of two-dimensional motion as though the sphere were moving along the center plane at 32 ft from the horizontal camera, parallel to the film plane.

A representative plot of these two-dimensional trajectories for each sphere (#1 - #17) is shown on Figures 4, 5, and 6 (one repeated trial of Sphere #3 is given on Figure 6). From the original, more detailed trajectory plots, the sphere speed along the assumed two-dimensional path was computed from consecutive or alternate-consecutive frames. The plot of some of these total speeds vs. net vertical displacement is given on Figures 4 and 5, corresponding to the trajectory plots. From the sort of data going into the speeds shown on Figures 4 and 5, the instantaneous C_D values were found, and the mean C_D and the RMS value of C_D fluctuations were ascertained for each trial. These summary data are plotted in the familiar C_D vs. R_d form on Figure 7. Note that in this instance the C_D values refer to the two-dimensional total speed and so for erratic spheres are somewhat smaller than C_D values based on mean vertical velocity. The points for any one sphere lie along a particular line having a -2 slope on this log-log plot of C_D vs. R_d, because of the velocity interrelation between C_D and R_d.

To check for the accuracy of data taking and data reduction, three completely independent data reductions of one trial (Sphere #14) were made and compared, and three trials of the same sphere were made and the results compared. The three data reductions yielded C_d values within 4 per cent of the mean value, and the three separate trials gave C_D values differing by about the same amount. These data variabilities are thus small enough so that the main summary results on the log-log plot of Figure 7 can be considered as showing meaningful gross relationships. Repeated tests of the same sphere would demonstrate the same general type of self-induced motion.

However, in the following data evaluation it must be remembered that (a) data of this type are rather variable (especially the cases with wide excursions), (b) in most cases only one run from each sphere type was reduced, and (c) there is some bias toward "regular" cases in the data through data selection since cases with very wide excursions could not be utilized due to the sphere's moving laterally beyond the field of view of the camera or too close or far from the camera.

Speed Fluctuation and Lateral Movement

The variability in along-the-path speed is shown on Figures 4 and 5 for ascending spheres, and is summarized for all spheres on Figure 7; the two-dimensional sphere trajectories are given on Figures 4, 5, and 6. The plotted data turned out to be generally consistent with the expectation that (a) the self-induced motions tend to be regular for any trials in the subcritical regime and for spheres with large roughness elements in the supercritical regime, and (b) the self-induced motions tend toward random wandering for smooth and small roughness spheres operating in the supercritical regime. For the regular motion cases the separate effects of roughness and RM are discussed in detail in later portions of this section.

For the heavy, descending spheres the short period speed fluctuations and lateral movements are apparently well attenuated, presumably from RM effects. In the subcritical regime the descents shown on Figure 6 were fairly vertical, but in the supercritical regime the descents all showed a strong net wandering. It is hypothesized that the high rotational inertia of the steel spheres either tends to maintain any slight initial rotation or tends to maintain the relative position of a minute surface feature; in the supercritical R_d regime this could maintain a lateral translation of the sphere. The orientation of lightweight buoyant spheres, on the other hand, would tend to couple to the motion and not dominate the motion at subcritical R_d.

For the 34 trials of buoyant spheres, a qualitative impression of the amount of net lateral motion can be derived from the observer notes. These notes include more cases than are depicted on the Figures, and include data on the larger 16 in. diameter sphere.

Spheres with large roughness elements: Most hit the surface within 1 ft of the centerline (one 12-in. diameter hit at 2 ft, another at 4 ft).

Spheres with small roughness elements: Most hit beyond the 7 ft opening radius, with a few within 3 ft.

Smooth spheres: The small subcritical 3.4 in. spheres and the large 16 in. spheres hit within 3 ft of the centerline. The other sizes (5.6 in., 10.5 in., 12 in.) hit at greater distances, most being beyond the 7 ft opening radius.

In summary, as would be expected, all the buoyant spheres with large roughness elements exhibited only regular motions and hence small net excursions. The spheres with small roughness elements had mostly large total motions, comparable to or slightly greater than those for smooth spheres. The subcritical spheres of any roughness gave small net excursions. In addition, the 16 in. diameter spheres gave small net excursions somewhat analogous to subcritical motions.

Mean C_D Values

On Figure 8 are sketched some suggested C_D - R_d curves which are reasonably consistent with the mean data of Figure 7 and which serve to illustrate the effects of separate factors. The Reference Curve on Figure 8 is the one suggested by MacCready and Jex (1964) to represent the C_D - R_d relation for a hypothetical "infinite mass" sphere having no self-induced motion. Additional data are presented for superpressure balloons on Figure 9. As discussed by MacCready and Jex (1964), the C_D - R_d curve of a sphere may have an abrupt jump in the critical R_d regime, the jump taking place along a -2 slope on a log-log plot, and in the region of this jump the C_D - R_d curve will have a different value depending on whether the curve relates to a sphere experiencing a decreasing R_d (as with an ascending balloon) or an increasing R_d. The curves on Figure 8 pertain to the speeds of spheres released from rest and thus reaching the particular R_d from lower R_d values. For simplicity the curves are drawn with no slope reaching -2. When relating them to C_D - R_d curves from ascending balloons, the possibility of doubled valued curves must be recognized. On Figure 8, omitting the four points for the spheres with large roughness elements, the four points at high R_d are well into the supercritical R_d regimes, the five points at low R_d are most likely in the subcritical regime, and the middle four points are probably just in the supercritical regime (judging from the low C_D values).

In the supercritical regime, the drag (and motions) of smooth and slightly rough spheres are similar. The drag coefficients are somewhat higher than the values given by the Reference Curve and the values found for spheres mounted rigidly in wind tunnels, presumably partially because of the additional energy required to accelerate the mass (sphere mass plus apparent mass) along the curved trajectory. The values are in keeping with those of Figure 9 and the balloons cited by MacCready and Jex (1964). The very rough sphere has high drag due to the drag of the roughness elements themselves and the thickening of the wake.

The critical R_d is moved toward lower R_d by the roughness which maintains a turbulent boundary layer. Thus, as shown on Figure 8, at a particular range of R_d the rough sphere can have a lower C_D than the other spheres since the rough sphere is at supercritical R_d while the smoother spheres are at subcritical R_d.

In the subcritical R_d regime, the C_D values tend to cluster around 0.4, considerably lower than the values, which were often about 0.8, at comparable R_d in the tank tests of MacCready and Jex (1964). A good portion of the discrepancy arises because the points on Figure 8 relate to local speed, while the data from the earlier tank tests were from the mean vertical speed. It is also possible that the sphere motions relating to these points on Figure 8 were not fully in the subcritical R_d regime.

Relative Mass Effects at Subcritical R_d

This set of experiments only treated two relative mass categories: light buoyant spheres, $0.037 < RM < 0.163$, and heavy spheres, $RM = 7.8$. As derived by MacCready and Jex (1964), other things being equal, the amplitude of a sphere zigzag motion in the subcritical regime may be expected to vary roughly as $\lambda(1 + 2\,RM)^{-1}$ where λ is the wavelength of the regular motion. This sort of factor derives simply from noting that the resistance to disturbance is related to the total effective mass (the sphere mass plus the apparent mass which is 1/2 the displaced fluid), while the disturbance strength is related to fluid mass. The derivation was made for zigzag motions, but similar reasoning can be applied to spiral motion also. MacCready and Jex estimated the constant of proportionality from water tank data giving

$$y_{max} \sim 0.2\ \lambda\ (1 + 2\ RM)^{-1} \qquad (1)$$

Noting that commonly $\lambda \sim 14D$, the above amplitude equations can be put in terms of diameter D:

$$\frac{y_{max}}{D} \sim 2.8\ (1 + 2\ RM)^{-1}, \qquad (2)$$

Thus for the buoyant spheres here

$$\frac{y_{max}}{D} \sim 2, \qquad (3)$$

while for the steel ball the motion would be an order of magnitude less:

$$\frac{y_{max}}{D} \sim 0.17. \qquad (4)$$

Therefore, the spurious short period motions would not be expected to be visible with the steel balls, but would be quite apparent for the buoyant 3.4 in. diameter balls. These expectations are in agreement with the observed motions, none being visible for the small steel balls, and about half a foot being observed for the smooth 3.4 in. diameter sphere. The 3.4 in. sphere with small roughness elements is shown, on Figure 5, to have somewhat larger lateral excursions. This sphere was not accurately spherical, and its center of mass did not coincide accurately with its center of buoyancy; it is hypothesized that the wavelength was established by a complex coupling between the vortex shedding and these physical features.

Preukschat (1962) has a plot of amplitude/diameter for various relative mass ratios for spheres of RM between 0.53 and 0.88 operating at subcritical R_d somewhat below those reported here. Equation (1) is in reasonable agreement with his data (with, of course, the expected scatter characteristic of any typical sphere motion data).

Motion at High R_d

Practical difficulties on this project limit the data available to study motions at high R_d. However, there were several movies taken from above showing the ascent of the 16 in. diameter smooth

sphere in the R_d regime around 1,600,000. These spheres exhibited an irregular motion which could be termed a crude spiral of amplitude about two sphere diameters. Although irregular, the motion was much more regular than that of the 5.6 in., 10.5 in., or 12 in. spheres. The three trials of 16 in. spheres exited from the water at only 1 ft , 1 ft , and 3 ft from the centerline. The exiting was at the end of about one complete spiral which seemed to begin after the sphere had risen about 1/3 of the tank depth.

A hint that the self-induced motion of spheres becomes smaller and more regular as R_d becomes very high is contained in some superpressure balloon ascent data previously obtained by Scoggins. These data are shown on Figure 2a, page 16, of the report by Stinson, Weinstein, and Reiter (1964). The figure depicts the horizontal wind speeds shown by serial ascents of these balloons at intervals of approximately one hour. Different balloon diameters were used, respectively 4 ft, 2 m, 8 ft, 4 ft, 2 m, 7 ft, 8 ft, 7 ft, and 7 ft. The amount of spurious motion can be seen in the scatter of the profile points (assuming the atmospheric situation to be relatively unchanging at least as regards turbulence). This motion pertains to net lateral movements not filtered out by 4-second averaging of balloon positions. The 7th ascent, with an 8 ft diameter balloon, shows that at the lowest altitudes and hence highest R_d ($R_d \sim 1,200,000$) the net self-induced motion was small. At higher altitudes and lower R_d, the self-induced motion began increasing, becoming comparable to the motions shown by the smaller balloons operating at lower (but still supercritical) R_d. The 3rd ascent, with the other 8 ft diameter sphere, does not show the same effect but does have less scatter all the way up than most of the 2 m and 7 ft diameter spheres. The different sphere sizes had different construction details and different numbers of gores, and there were also minute differences between individual versions of the same diameter. Since the details of the self-induced motions in the supercritical regime are so dependent on tiny surface features of the balloons, the quantitative interpretation of the self-induced motions shown by the serial ascents should not be carried too far, but the one case of the 7th ascent does suggest the tendency toward regular motion at very high R_d as observed in the water tank.

Figure 9 presents C_D - R_d plots provided by Scoggins for the balloons of the series. These data were derived assuming that the average drag balances the average buoyancy. A complete plot of C_D - R_d variation of the 8 ft diameter balloon is

shown, together with the critical R_d points for the other spheres (except for the second 8-foot diameter balloon for which data were missing around the critical R_d point). The C_D - R_d curve for the ascending balloon is not inconsistent with the points shown on Figure 7 for the smooth spheres. The variation of critical R_d points for the various balloon types emphasizes the great sensitivity of the transition to small variations of sphere surface details. The critical R_d points are at lower R_d for the smaller balloons, which might be the result of greater relative roughness on the surface of the smaller balloons.

Roshko (1961) reports that with a circular cylinder the flow does change from the random wake with low drag in the low supercritical regime to a more regular wake with higher drag at a high supercritical regime (the transition being at $R_d \sim 3,500,000$). The physical mechanisms associated with classical sub- and supercritical R_d regimes for cylinders are somewhat analogous to the flows around spheres. It seems likely that there is a similar analogy between Roshko's high supercritical regime and the reappearance of "regular" motion suggested by the 8-foot diameter sphere in the atmosphere and the 16-inch diameter buoyant sphere in the water.

At subcritical R_d the boundary layer for a cylinder separates while still laminar, and does not become turbulent until too far back to reattach. At supercritical R_d the cylinder boundary layer separates while laminar, then becomes turbulent and reattaches further back on the cylinder, resulting in a small wake. At high supercritical R_d the cylinder boundary layer has its transition to turbulence ahead of separation and the wake becomes larger than at supercritical R_d, large enough to take on the sort of double vortex sheet configuration which has a tendency to evolve toward the classic Karman vortex street usually associated with the subcritical R_d regime. In the sphere case, the boundary layer and wake size configuration are presumed analogous to the cylinder case, with the release of irregular vortex loops instead of the generation of the Karman vortex street.

Characteristics of the Transient Motions

The self-induced motions photographed in the previous and present water tank studies seem to show some impulsive motion taking place every 5 to 10 sphere diameters. In the subcritical regime these impulses appeared to be regularly alternating, with the result being regular motion of the sphere and no net gross wandering. In the supercritical regime these impulses apparently are randomly oriented, and the lateral wandering can be expected to occur. The impulses

can to some extent be observed in the speed fluctuations shown by all the smooth and small roughness spheres on Figures 4 and 5. For spiral sphere motion,the strength of the impulses may be somewhat reduced, and for some particularly smooth spiral motion they might possibly even be missing, with a narrow pair of vortices spiraling out smoothly.

The distances (I-I) between significant lateral accelerations of the buoyant spheres were estimated from the vertical camera. The results are given on Figure 10, where the ordinate is $2(SS) = D\left[(I\text{-}I)\right]^{-1}$, the reciprocal of the distances in terms of diameters. When the accelerations are in alternating directions, then the dominant wavelength λ will be $2(I\text{-}I)$ and $(SS) = D\left[2(I\text{-}I)\right]^{-1} = D/\lambda$. For this reason (SS) is considered a "Sphere Motion Strouhal" number, the number analogous to the conventional Strouhal number for the diameter/wavelength ratio for the flow behind a cylinder at subcritical R_d (for which the Strouhal number is ~ 0.21). Figure 10 gives $(SS) \sim 0.07$ ($\lambda \sim 14\ D$ for the regular motion cases).

Tunnel measurements with fixed spheres at low subcritical R_d in water or air have helped to illuminate the impulse process. The discussion by Goldstein (1938), pp 577-579, notes:

(a) At $R_d > 100$ an "oscillating disturbance of the surface of the vortex-ring becomes visible, with the result that successive portions of its substance are discharged downstream at regular intervals".

(b) "Rosenhead has suggested the only possibility is a sequence of irregularly shaped vortex-loops."

(c) Photographs from the wake of a circular disk by Stanton and Marshall show the irregularly shaped vortex-rings at definite intervals at higher R_d.

Photographs of sphere wakes by F.H. Abernathy (private communication) and Lehman (1964) show vortex-loops being regularly released in the wake, in alternating directions.

When the sphere is permitted to move freely, the wake and the sphere motion can be expected to interact to establish a final wavelength of motion. The previous report showed, with considerable scatter, that $\lambda \sim 14\ D$, and the present study is in reasonable agreement. For lower R_d, Preukschat (1962) found $\lambda \sim 15\ D$, again with

the expected scatter. His data suggest that λ/D increases with increasing RM for buoyant spheres. It seems logical that the wavelength would depend somewhat on RM since this relates to the coupling of the motion to the wake. In the atmosphere, a trajectory shown by Scoggins (1964, 1965) for a Jimsphere, a 2 m balloon with numerous large roughness elements, gave $\lambda \sim 14D$. At very low R_d, say around 1000, the wake becomes regular, and the self-induced motion dies out. More detailed studies will likely show systematic variations of λ/D or $(I-I)/D$ with R_d and roughness.

Careful examination of the present film records suggested that there were also small, high frequency, impulsive motions taking place in addition to the larger motions. The data resolution was not sufficient to permit these to be examined in any detail. Winny (1932) observed that the average vortex frequency on the surface of a sphere is about four times as high as in the wake. Probably various frequencies are involved in the impulsing, causing significant sphere motion. The dominant frequencies will tend to be at low frequencies since the sphere response can then be large, and the final dominant frequency will be a function of the interaction between sphere motion and the wake flow. Further conjecture about the transient flow phenomena from the limited data of this study does not seem warranted here.

These experiments showed that at supercritical R_d the roughness elements did not have an effect in smoothing the motion unless the elements were large. When large elements were used, the motion became regular and analogous to the subcritical R_d regime. For the rough surface ascending supercritical spheres of this study, the motion amplitudes as shown on Figures 4 and 5 are regular and small. Atmospheric tests suggest that, once there are enough large roughness elements to assure regular motion, then the amplitude of the regular motion is decreased as the number of roughness elements increases. For example, plots presented by Scoggins (1964) of 4-second averaged winds at low altitude for 2 m balloons with 0, 90, or 270 cone-shaped drinking cups attached gave RMS speed variations (estimated roughly from the plots) of 2 m/s, 1 m/s, and 0.3 m/s, respectively (the last number perhaps depending mostly on the atmospheric turbulence). At 10 km, at lower R_d, the values were 1.7 m/s, 0.5 m/s, and 0 m/s.

SECTION V. CONCLUSIONS AND RECOMMENDATIONS

In summary, the sort of flow regimes found for cylinders (see, for example, Goldstein, 1938, and the recent review by Morkovin, 1964) appear to have direct analogs in the flow around spheres. The coupling between the flow and the sphere motion complicates the picture, but probably does not upset the basic flow regime. Water tank tests do provide data which are consistent with measurements on spherical balloons rising through the atmosphere.

Some questions to be answered in further studies are:

What determines whether the sphere motion at subcritical R_d is zigzag or spiral? Are there periodic motion impulses even in the true spiral mode? What are the exact RM effects in spirals and zigzags, and how do the amplitudes and wavelengths vary with R_d, RM, and roughness?

Does the self-induced motion really become an irregular spiral at high supercritical R_d?

For the operational application of spheres for high resolution wind soundings, how do the magnitudes of the self-induced lateral and longitudinal fluctuations vary with size and number of surface roughness elements at supercritical R_d? For lower resolution wind soundings, how many roughness elements are needed to assure that the self-induced motion becomes regular?

The above questions can be answered by measurements of the type reported here, but made in a more quantitative fashion. However, it should be recognized that programs of more basic nature must be developed to explain the underlying causes of the phenomena in a satisfactory manner. The most fundamental problem seems to be to investigate the wake generation and wake configuration for unconstrained spheres of low RM at subcritical, supercritical, and high supercritical R_d.

ACKNOWLEDGMENTS

The authors are indebted to Mr. Henry Jex of Systems Technology, Inc. and Dr. Anatol Roshko of California Institute of Technology for many helpful suggestions throughout this study, and to Mr. J. R. Scoggins of NASA, MSFC, Huntsville, for providing data on atmospheric tests, as well as helping through various discussions.

REFERENCES

Goldstein, S., 1938: (Editor), Modern Developments in Fluid Dynamics, Volume II. Oxford, England, Clarendon Press, 702 pages.

Lehman, August F., 1964: Some Cavitation Observation Techniques for Water Tunnels and a Description of the Oceanics Tunnel. Oceanics Inc., New York.

MacCready, P.B., Jr., and H.R. Jex, 1964: Study of Sphere Motion and Balloon Wind Sensors. Final Report to NASA, Huntsville, Ala., Contract NAS 8-5294. NASA TM X-53089

Morkovin, M.V., 1964: Flow Around Circular Cylinder - A Kaleidoscope of Challenging Fluid Phenomena. Proc. of Symp. on Fully Separated Flows, ASME Fluids Engineering Div. Conf. at Philadelphia, May 1964. Publ. by Am. Soc. of Mechanical Engineers (Lib. of Cong. No. 64-21649).

Preukschat, A.W., 1962: Measurement of Drag Coefficients for Falling and Rising Spheres in Free Motion. Aeron. Eng. Degree Thesis, Calif. Inst. of Tech.

Roshko, Anatol, 1961: Experiments on the Flow Past a Circular Cylinder at Very High Reynolds Number. J. Fluid Mech., 10, 3, 345-356.

Scoggins, J.R., 1964: Aerodynamics of Spherical Balloon Wind Sensors. J. Geophys. Res., 69, 4, 591-598.

Scoggins, J.R., 1965: Spherical Balloon Wind Sensor Behavior. J. Appl. Meteor., in press.

Stinson, J. R., A.I. Weinstein, E.R. Reiter, 1964: Details of Wind Structure from High Resolution Balloon Soundings. Revision of Final Report to NASA, Huntsville, Ala., Contract NAS 8-5294. NASA TM X-53115

Winny, H.F., 1932: Vortex System Behind a Sphere Moving Through Viscous Fluid. A.R.C. Reports and Memoranda No. 1531, T. 3305.

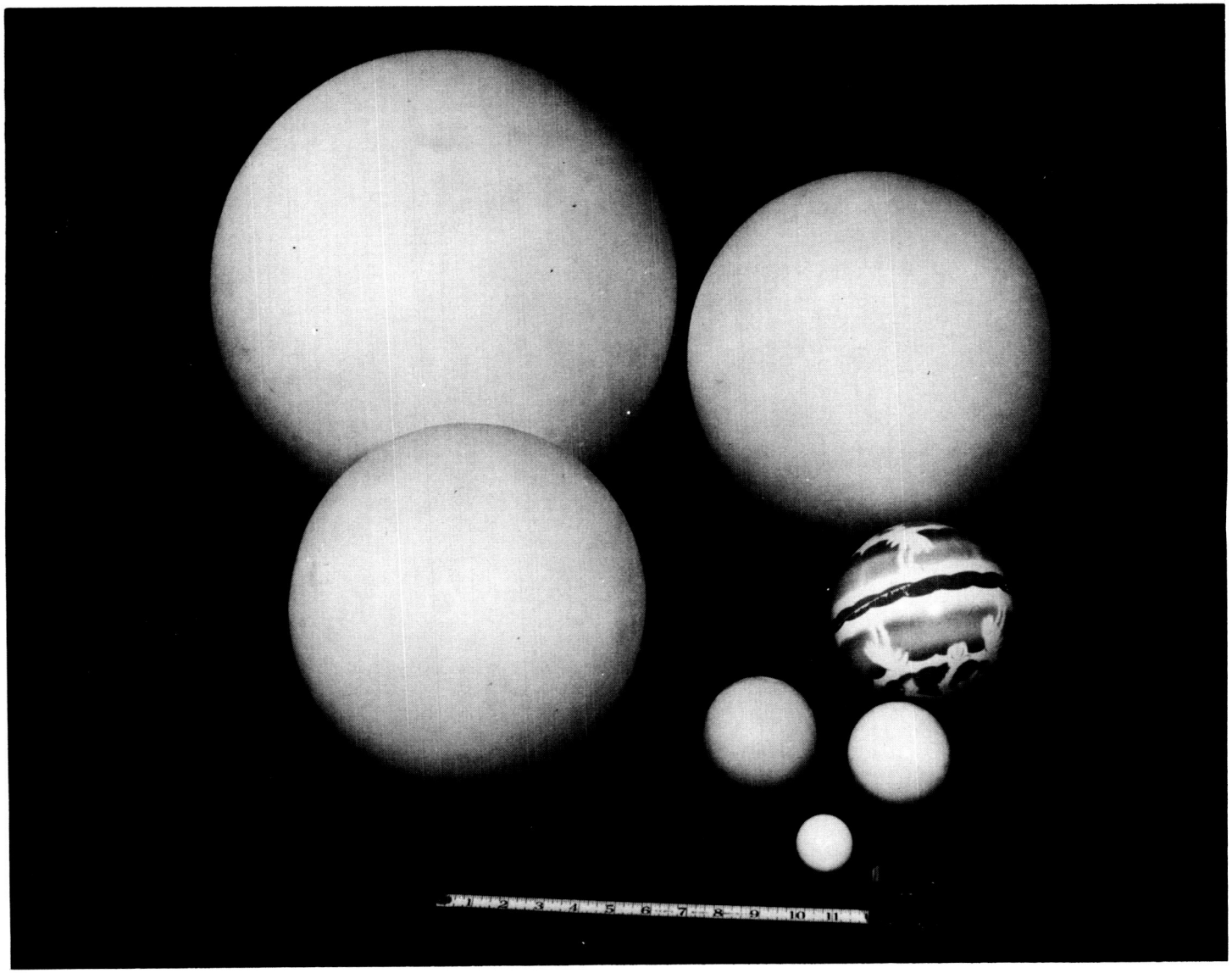

FIGURE 1. RELATIVELY SMOOTH SPHERES (#1, 5, 6, 9, 12, 15, 18)

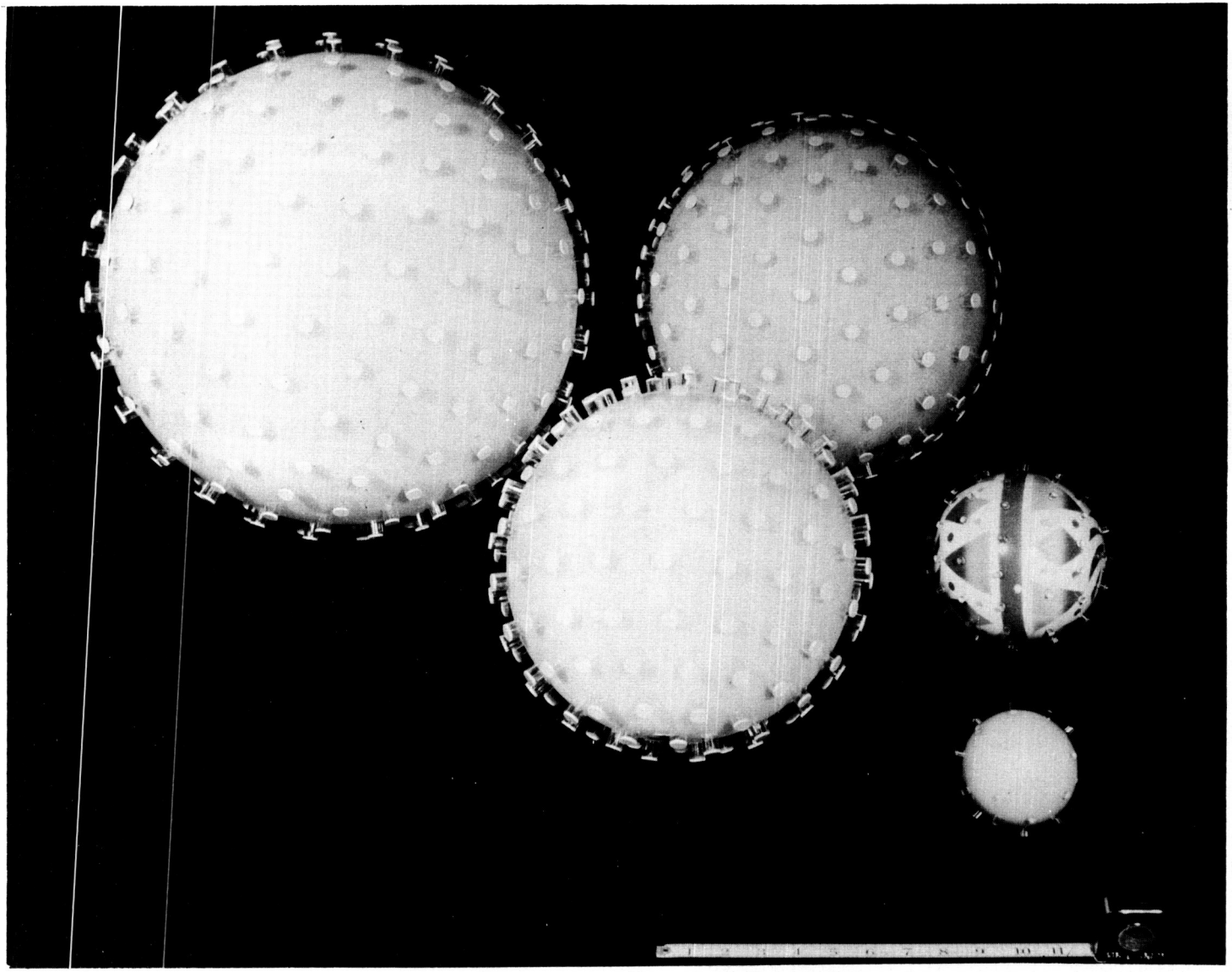

FIGURE 2. SPHERES WITH LARGE ROUGHNESS ELEMENTS (#8, 11, 14, 17, 19)

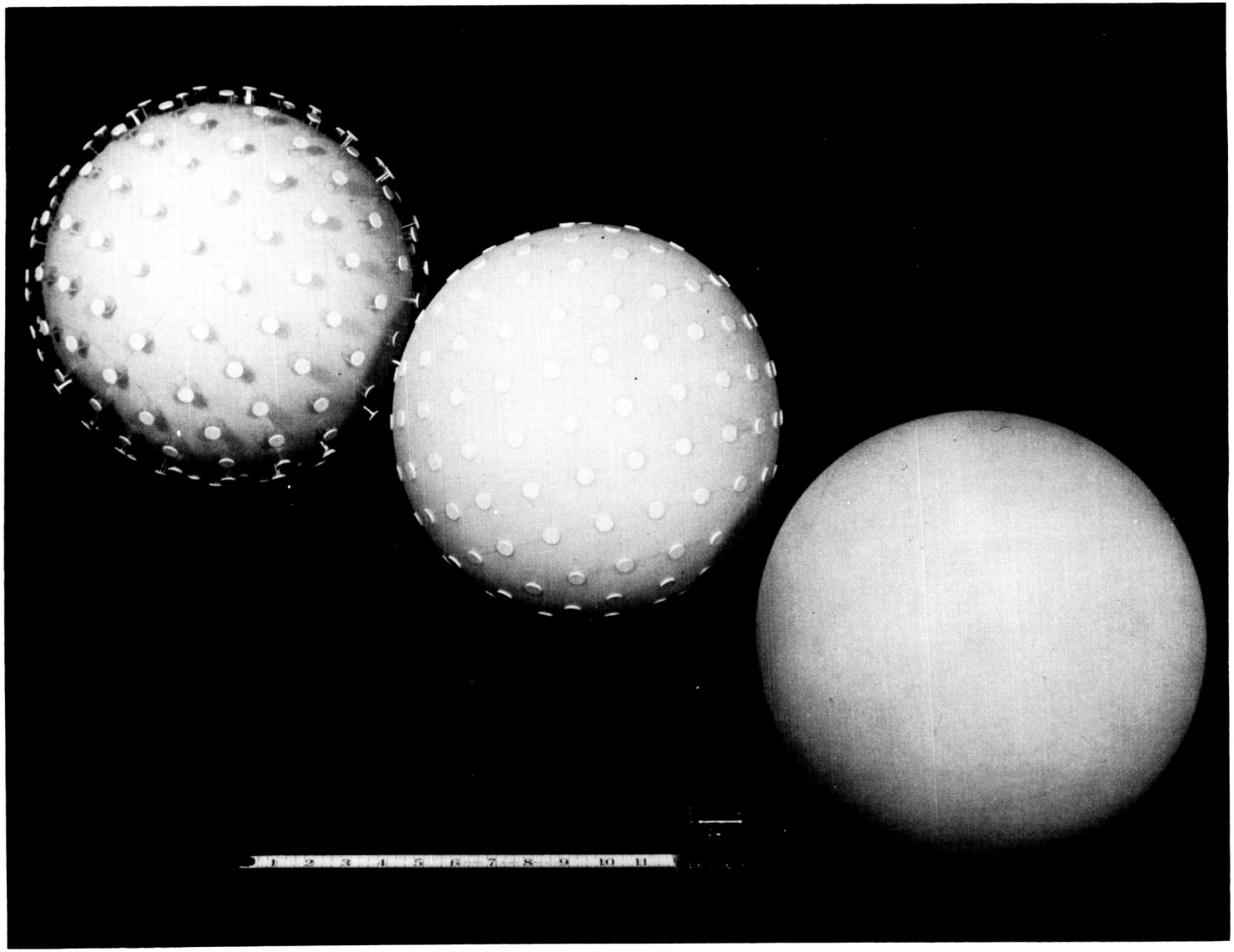

FIGURE 3. THE THREE ROUGHNESSES, L, S, AND N (SPHERES #15, 16, 17)

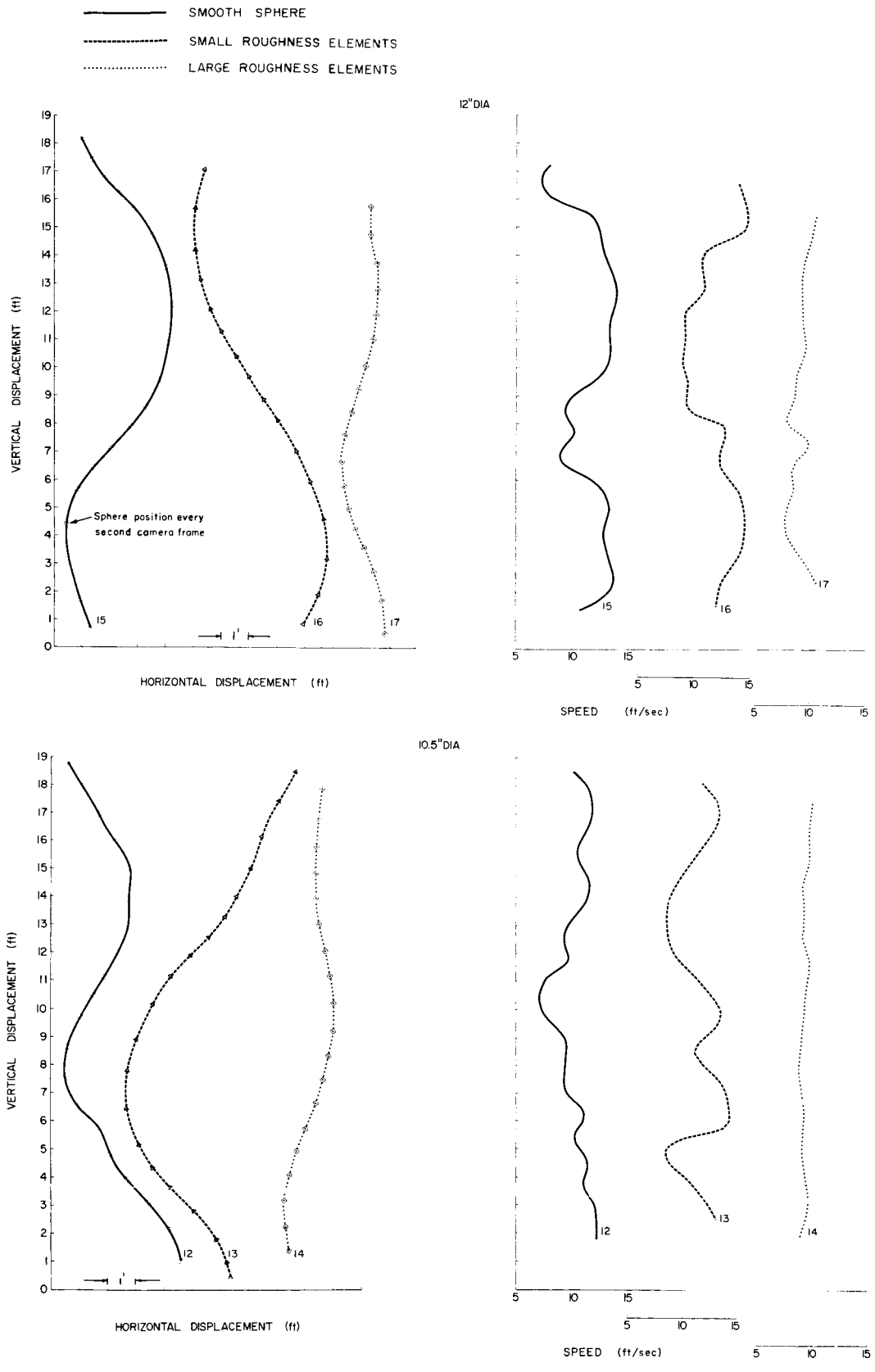

FIGURE 4. TRAJECTORY AND SPEED VS. VERTICAL DISPLACEMENT, ASCENDING SPHERES (12 IN. AND 10.5 IN., SUPERCRITICAL R_d)

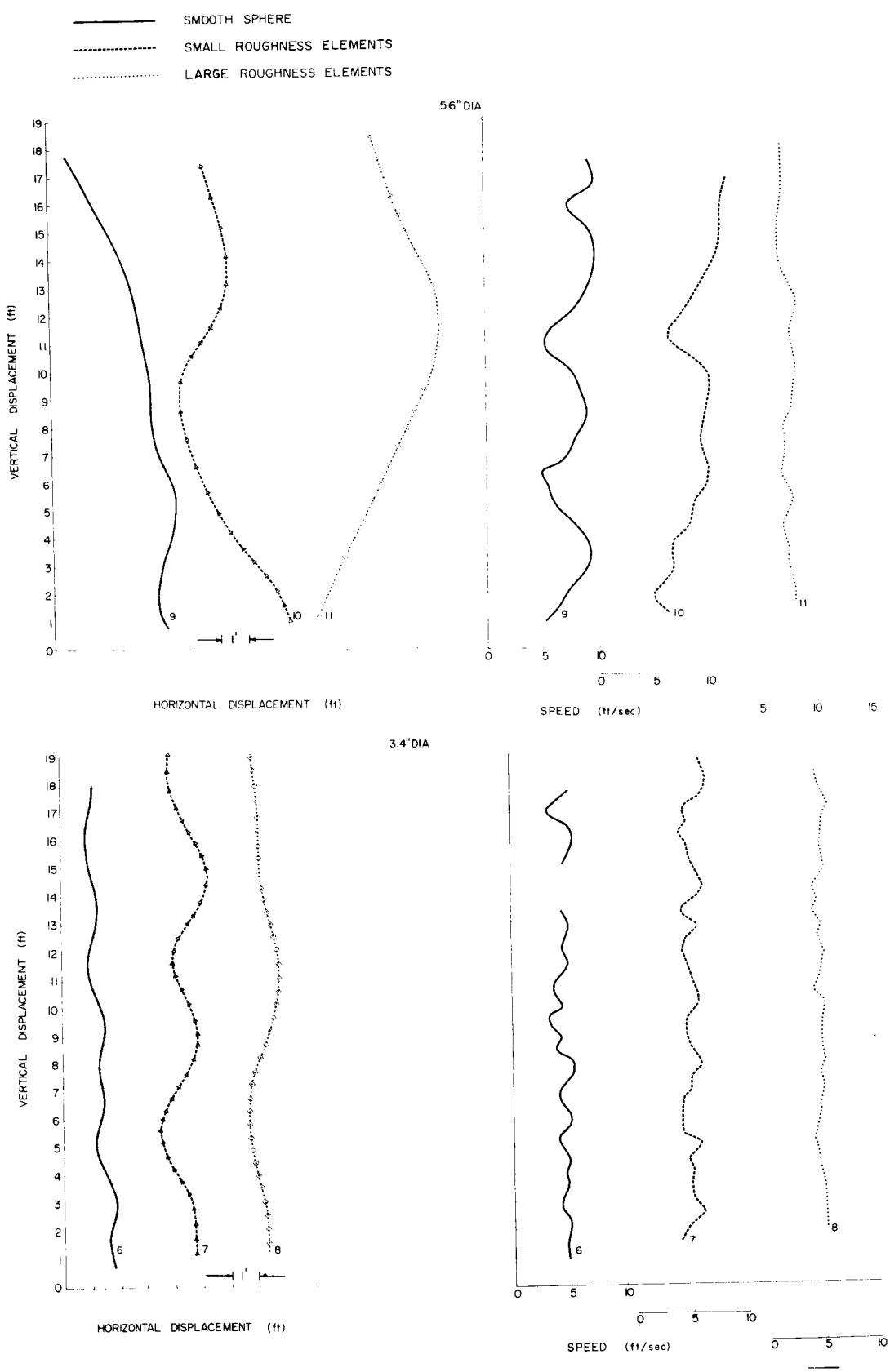

FIGURE 5. TRAJECTORY AND SPEED VS. VERTICAL DISPLACEMENT, ASCENDING SPHERES (5.6 IN. SUPERCRITICAL R_d, 3.4 IN. SUBCRITICAL R_d)

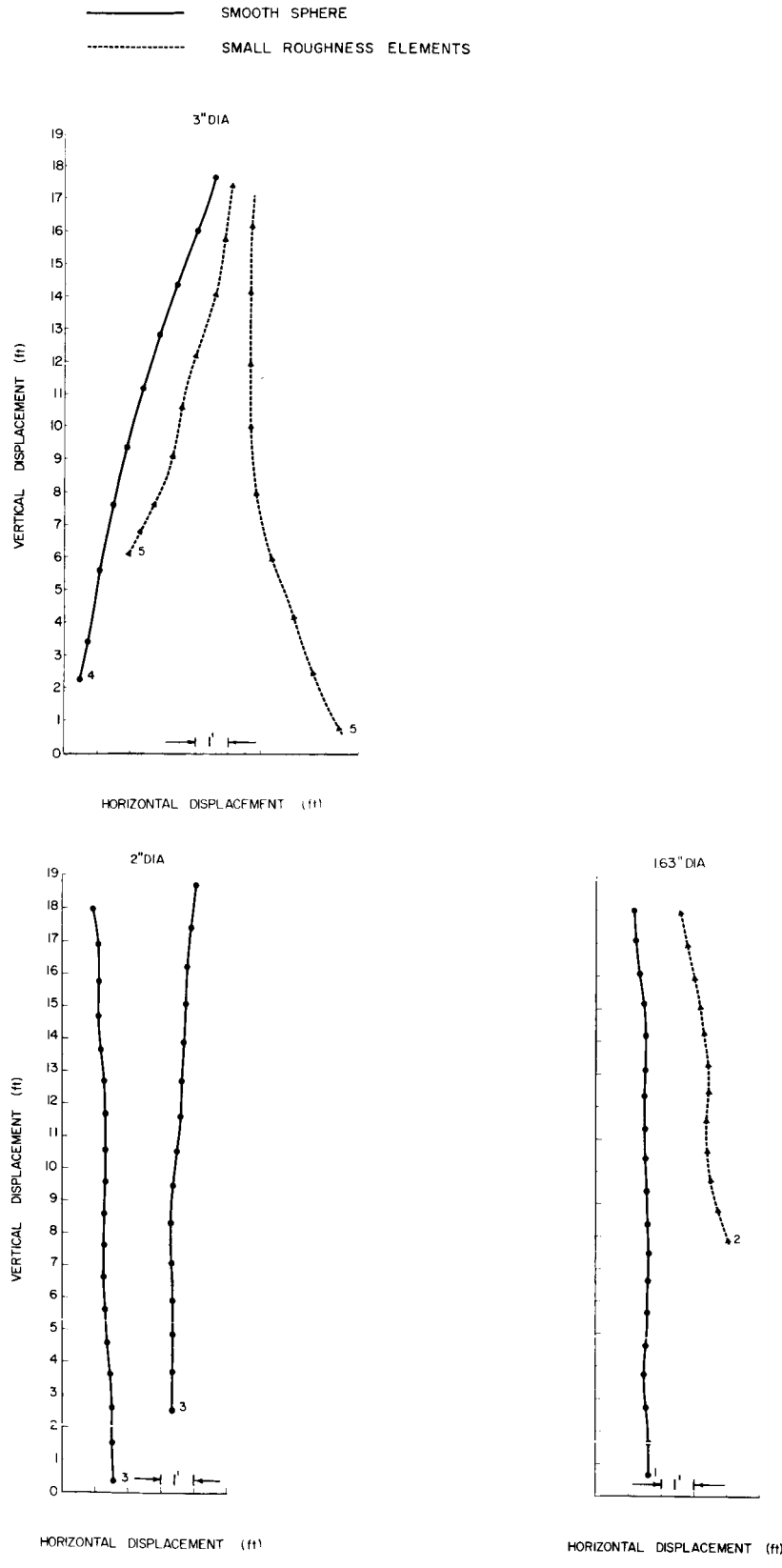

FIGURE 6. TRAJECTORY, DESCENDING SPHERES (3 IN. SUPERCRITICAL R_d, 2 IN. AND 1.63 IN. SUBCRITICAL R_d)

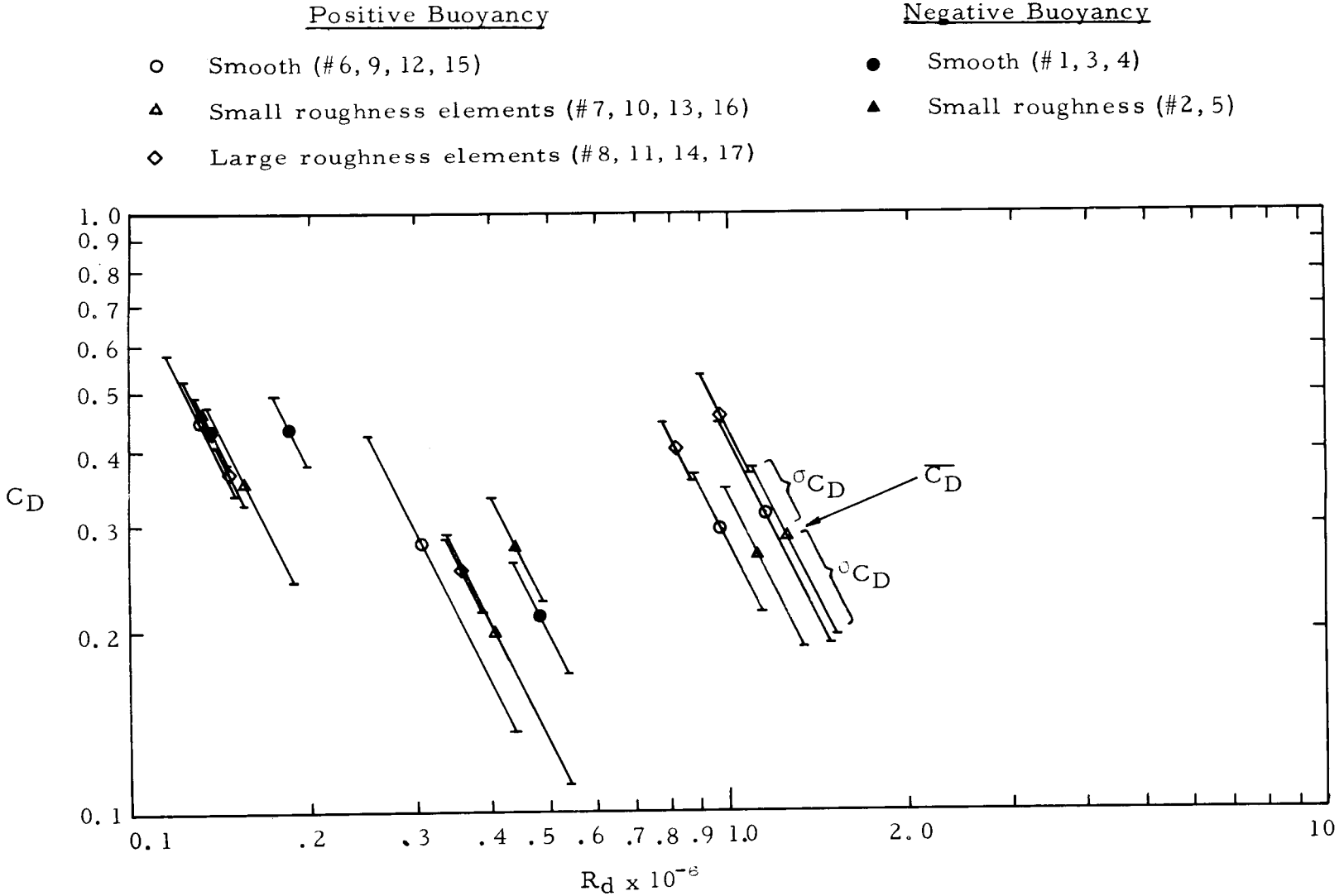

FIGURE 7. SUMMARY OF C_D VS. R_d AND C_D VARIABILITY (BASED ON LOCAL TWO-DIMENSIONAL SPEED)

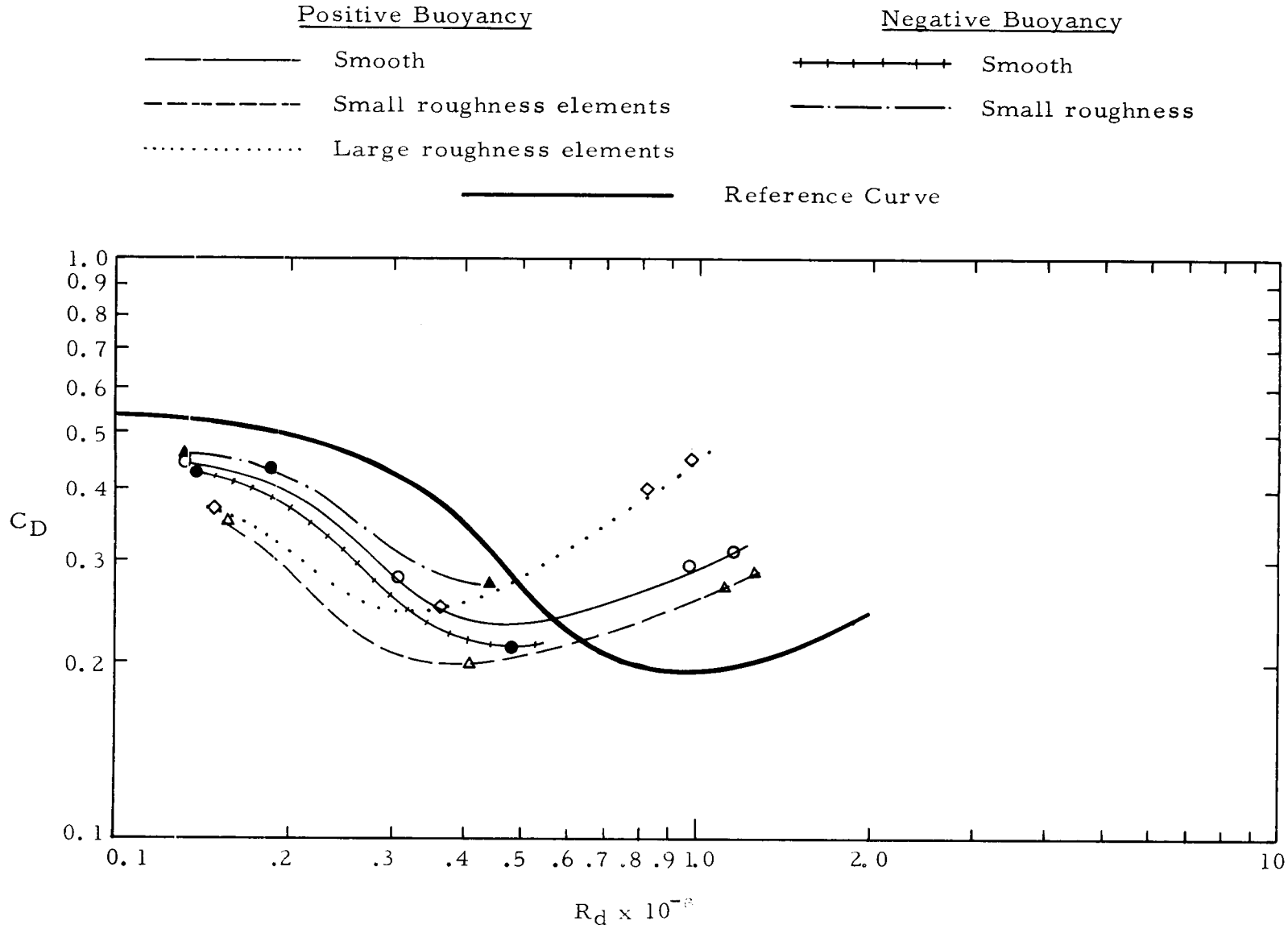

FIGURE 8. SUGGESTED C_D VS. R_d RELATIONS FOR VARIOUS SPHERE TYPES

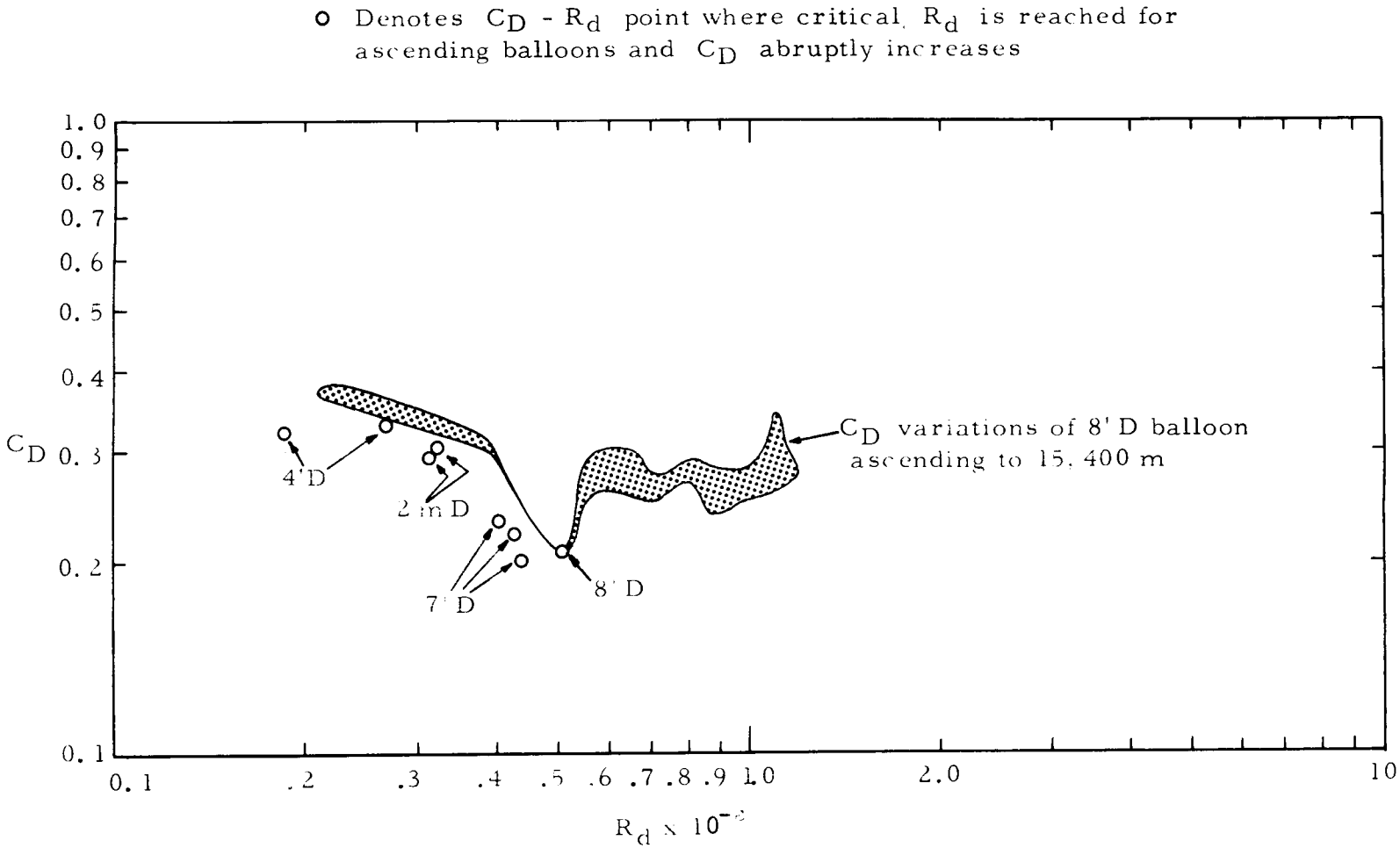

FIGURE 9. C_D VS. R_d FOR SOME SUPERPRESSURE BALLOONS

DISTRIBUTION

MS-IP

Dep Dir Technical
Dr. Rees

R&D Operations
Mr. Weidner
Mr. Dannenburg

Aero Laboratory
Dr. Geissler
Mr. O. C. Jean
Mr. R. Horn
Mr. C. Baker
Mr. J. Lindberg
Mr. L. Stone
Mr. T. Reed
Mr. J. de Fries
Mr. L. McNair
Mr. W. W. Vaughan (5)
Mr. J. R. Scoggins (40)
Mr. J. W. Kaufman
Mr. W. K. Dahm
Mr. O. E. Smith
Mr. M. Rheinfurth

Research Projects - DIR

TEST-DIR

LVO-DIR

Kennedy Space Center
Dr. Knothe
L/Col. Patrone
Mr. D. Collins
Mr. A. Taiani
Dr. R. H. Bruns (3)

P&VE Laboratory
Mr. R. Hunt
Mr. N. Showers

Army Missile Command
Library
Dr. Essenwanger

Langley Research Center (NASA)
Langley Field, Virginia
H. B. Tolefson (2)
Vernon Alley
R. M. Henry
Library
Wilmer H. Reed, III (2)

Wallops Station (NASA)
Wallops Island, Virginia
Mr. Spurling

Goddard Space Flight Center (NASA)
Greenbelt, Maryland
Mr. W. Stroud

NASA Headquarters
Washington, D. C.
Tracking & Data Acquisition Office
Mr. T. Buckley
Office of Advanced Research & Technology
Mr. Rhode, RVA
Mr. D. Gilstad, RV-2 (2)
Office of Space Sciences & Applications
Dr. M. Tepper (2)

Air Force Cambridge Research Laboratories, Code: CREW
L. G. Hanscom Field
Bedford, Massachusetts
Mr. N. Sissenwine
Mr. R. Leviton
Mr. R. Slavin
Lt. Dan Reid
Mr. Gringorten
Library

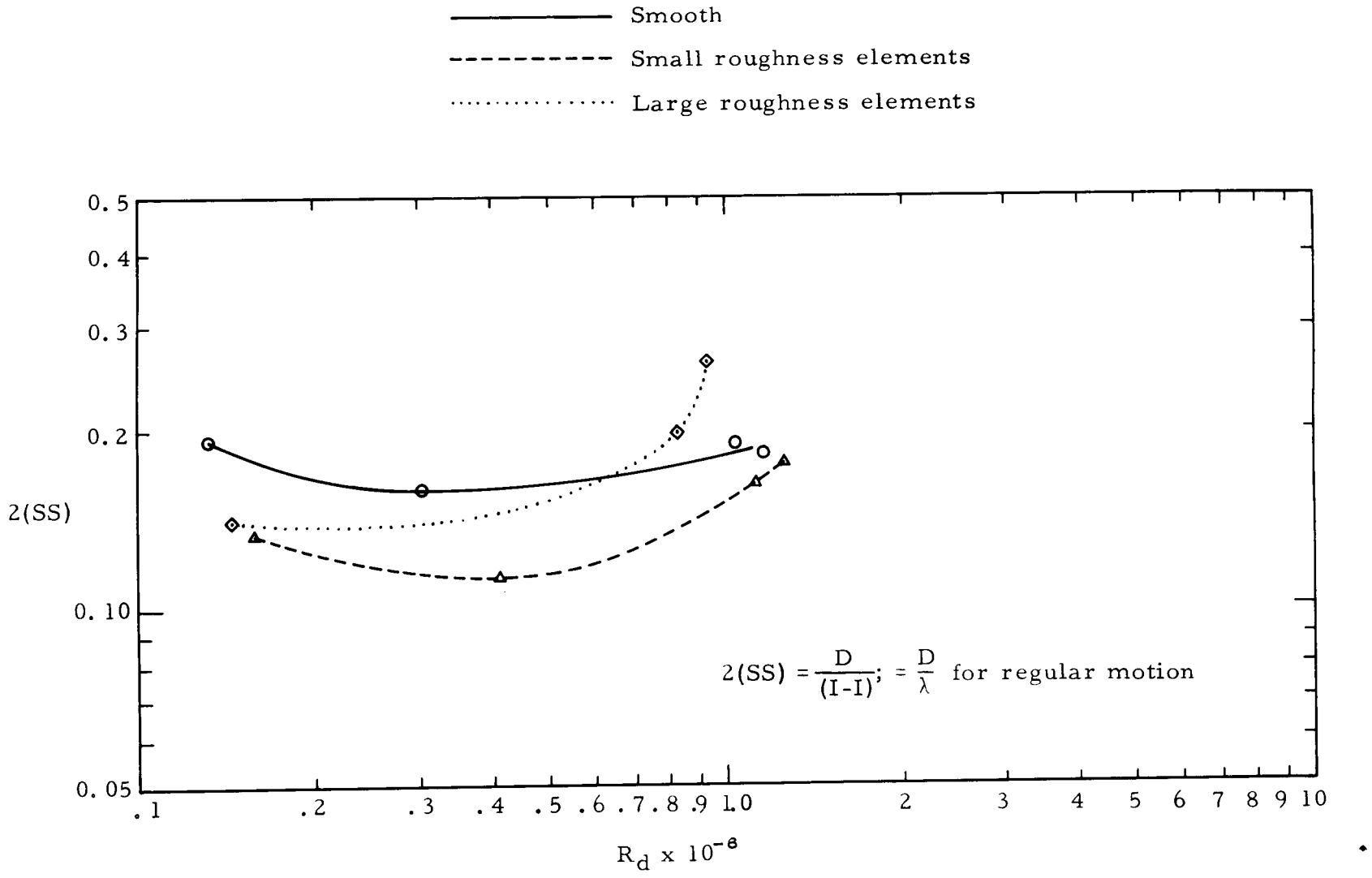

FIGURE 10. SPHERICAL STROUHAL NUMBER FOR VARIOUS SPHERES

DISTRIBUTION (CONT'D)

Commander (2)
Air Weather Service
Scott Air Force Base, Illinois

Air Force System Command (2)
Code SCWTS
Andrews Air Force Base
Washington, D. C. 20331

Mr. George Muller
Air Force Flight Dynamic Lab.
Air Force System Command
Wright-Patterson AFB, Ohio

Mr. William Elam
Bellcomm, Inc.
1100 17th Street, N.W.
Washington, D. C.

Air Force Systems Command
Space System Division
Air Force Unit Post Office
Los Angeles, California

Meteorological & Geoastrophysical
Abstracts
P. O. Box 1736
Washington, D. C.

Mr. Richard Martin
General Dynamics/Astronautics
San Diego, California

Meteorology Research, Inc.
2420 N. Lake Avenue
Altadena, California
Dr. Paul B. MacCready, Jr. (25)
Mr. Robin E. Williamson (25)

Systems Technology, Inc.
Inglewood, California
Mr. Henry Jex

Dr. David P. Hoult
Dept. Aeronautical Engineering
Pennsylvania State University
University Park, Pennsylvania

Dr. Hans A. Panofsky
Department of Meteorology
College of Mineral Industries
Pennsylvania State University
University Park, Pennsylvania

White Sands Missile Range
Missile Meteorology Group
Mr. W. Webb
Mr. H. Rachele

NASA-Manned Spacecraft Center
Houston, Texas
Mr. D. Wade
Technical Library

Cornell Aeronautical Lab., Inc.
Buffalo, New York
Mr. R. Pilie'
Dr. R. Rogers (3)

G. T. Schjeldahl Company
Northfield, Minnesota
Mr. C. V. Eckstrom (4)

Office of Research and Grants
NASA Headquarters
Washington, D. C.
ATTN: Dr. Smull (2)

Dr. Robert White, Chief (3)
U. S. Weather Bureau
Washington, D. C.

Director National Center for
Atmospheric Research
Boulder, Colorado

DISTRIBUTION (CONT'D)

Dr. Helmut Heinrich
Dept. Aeronautical Engineering
University of Minnesota
Minneapolis, Minnesota

MS-IPL (8)
MS-H
HME-P
CC-P

Scientific & Technical Information
Facility (2)

Attn: Nasa Representative (S-AK/RKT)
P. O. Box 5700
Bethesda, Maryland